

Inertial Range Scaling in Rotations of Long Rods in Turbulence

Shima Parsa and Greg A. Voth*

Department of Physics, Wesleyan University, Middletown, Connecticut 06459, USA

(Received 19 April 2013; published 15 January 2014)

We derive a scaling relationship for the mean square rotation rate of rods with lengths in the inertial range in turbulence: $\langle \dot{p}_i \dot{p}_i \rangle \propto l^{-4/3}$. We present experimental measurements of the rotational statistics of neutrally buoyant rods with lengths $2.8 < l/\eta < 72.9$, and find that the measurements approach the predicted scaling. The approach to inertial range scaling is shown to be more complex than anticipated with an overshoot and approach to the scaling from above. For all rod lengths, the correlation time of the Lagrangian autocorrelation of the rotation rate scales as the turnover time of the eddies of the size of the rod. Measuring rotational dynamics of single long rods provides a new way to access the spatial structure of the flow at different length scales.

DOI: 10.1103/PhysRevLett.112.024501

PACS numbers: 47.27.Gs, 47.55.Kf

The dynamics of particulate material in fluid flows is important in a broad range of problems in nature [1,2] and industry [3]. Extensive work on small spherical particles has revealed a rich phenomenology with applications in cloud physics and sedimentation [4–7]. Studies of particle dynamics have also provided new insights into turbulence itself since a Lagrangian reference frame minimizes sweeping and provides the natural frame for analyzing the time evolution of turbulence [6]. However, connecting a Lagrangian perspective with traditional insights about inertial range power law scaling has been difficult because statistics of changes over Lagrangian time intervals do not show clear inertial range scaling at accessible Reynolds numbers [8]. Rigid particles with lengths that extend into the inertial range provide a powerful tool to explore turbulence dynamics at a fixed scale in an advected reference frame.

For large spheres, it has been found in both experiments [9–12] and numerical simulations [13,14], that the acceleration variance scales with the sphere diameter approximately as $\langle a^2 \rangle \sim d^{-2/3}$ for d in the inertial range [9–12]. This result can be obtained by dimensional arguments simply assuming that the sphere terminates the cascade at its diameter [9]. It can also be derived from the inertial range form of the pressure structure function or the acceleration correlations [10–12]. Measuring the acceleration of large spheres provides access to the statistics of the turbulence at scales equal to the size of the spheres using only single particle measurements. Recent experimental work by Volk *et al.* [12] finds that the $d^{-2/3}$ scaling is not exact and proposes a scaling of $d^{-0.81}$ by including intermittency in the pressure structure function.

In this Letter, we study the rotations of rods with lengths that extend into the inertial range. Measurements and simulations of small rodlike particles have shown preferential alignment with the velocity gradients of the flow [15,16] and this alignment suppresses the measured rotation rate

in turbulent flows [17,18]. A wide range of experimental and numerical studies have explored the dynamics of neutrally buoyant small rods and fibers in different flows [19–23]. Only a few studies have focused on the dynamics of long rods in turbulence, where rod length spans over many times η , the Kolmogorov length scale [17,24]. Using numerical simulations and slender body theory, Shin and Koch [17] studied the translational and rotational dynamics of long fibers in turbulent flow at Taylor Reynolds number up to $R_\lambda = 53.3$. Among other things they show how the mean square rotation rate decreases as rods become longer than the tracer limit and identify the key role played by alignment of rods.

For large rodlike particles, the analytical theory to determine particle motion given the fluid fields can be done much more rigorously than for large spheres. For spheres, Faxén corrections can be used to extend point particle models to describe large spheres [25], but these models have difficulties when particles are much larger than η [13]. For rods, Olson and Kerekes [24] calculated the rotational velocity of fibers by treating them as slender bodies composed of many sections smaller than η which are hydrodynamically independent. For a neutrally buoyant fiber of length l , the rotation rate is

$$\dot{p}_i = \frac{12}{l^3} \int_{-l/2}^{l/2} (\delta_{ij} - p_i p_j) u_j(r) r dr, \quad (1)$$

where \mathbf{p} is the orientation unit vector of the fiber and \mathbf{u} is the turbulent velocity at points along the fiber [17]. If the orientation of a rod is uncorrelated with the velocity field in Eq. (1), then the mean square rotation rate of randomly oriented long rods is [24]

$$\langle \dot{p}_i \dot{p}_i \rangle = \frac{48 \bar{u}^2}{l^3} \int_0^l \left[1 - 3 \frac{r}{l} + 2 \left(\frac{r}{l} \right)^3 \right] R_{NN}(r) dr, \quad (2)$$

where \tilde{u}^2 is the rms velocity of the fluid flow and $R_{NN}(r)$ is the fluid transverse velocity correlation function at separation distance of r . Shin and Koch [17] show that Eq. (2) is in good agreement with their simulations for the case of randomly oriented rods.

We introduce a scaling for the mean square rotation rate of rods with lengths in the Kolmogorov inertial range. This scaling can be obtained either from dimensional arguments or from Eq. (2). The rotation rate has dimensions of inverse time, so for tracer rods it scales with the Kolmogorov time scale, $\langle \dot{p}_i \dot{p}_i \rangle \sim \tau_\eta^{-2}$. Assuming that long rods are only rotated and aligned by eddies close to their size, the mean square rotation rate for rods at length scale l will scale like τ_l^{-2} , where τ_l is the time scale of eddies of size l . In the inertial range, the time scale τ_l can be defined as $\tau_l = l/u_l = l/(l\langle\epsilon\rangle)^{1/3}$, where u_l is the velocity at length l , and $\langle\epsilon\rangle$ is the mean energy dissipation rate. This dimensional argument gives $\langle \dot{p}_i \dot{p}_i \rangle \sim l^{-4/3}$ for l in the inertial range.

The same $l^{-4/3}$ scaling can be obtained using Eq. (2), with the additional benefit that the coefficient can be determined in terms of known parameters. In homogeneous isotropic turbulence, the transverse correlation function in the inertial range is $R_{NN}(r) = 1 - (2/3\tilde{u}^2)C_2(\langle\epsilon\rangle r)^{2/3}$, where C_2 is an approximately universal constant [26,27], so in the inertial range

$$\frac{\langle \dot{p}_i \dot{p}_i \rangle}{(\langle\epsilon\rangle/\nu)} = \frac{108}{35} C_2 \left(\frac{l}{\eta}\right)^{-4/3}, \quad (3)$$

where ν is the kinematic viscosity. Here we use the fact that only scales near the length of the rod contribute to the rotation rate in Eq. (2) so that in the high Reynolds number limit the inertial range form of the structure function can be used for all r .

We have performed a series of experiments to measure the rotation of rods in three-dimensional turbulence for rod lengths that extend from the dissipation range well into the inertial range to explore whether an $l^{-4/3}$ scaling range exists. We measure neutrally buoyant rodlike particles with lengths ranging from 2.8η up to 72.9η in a turbulent flow between oscillating grids [28]. The rods are nylon thread with a diameter of 0.2 mm and are cut to different lengths ($l = 1, 3, 6.8, 15.2$ mm). All particles are dyed fluorescent for better detection. The rotational dynamics of rods are measured using stereoscopic images from four high speed cameras [18]. The detection volume is illuminated with four laser beams. This has nearly removed a limitation in earlier experiments [18] where the probability of detecting a particle depended on the orientation of the particle with respect to the laser beam. The number density of rods is very small so particle-particle interactions are negligible. The particle concentration is 0.025 cm^{-3} for 1 mm rods, and 0.0075 cm^{-3} for the longest rods at 15.2 mm.

TABLE I. Table of flow parameters: $R_\lambda = (15\tilde{u}L/\nu)^{1/2}$, Taylor Reynolds number; $\tilde{u} = (u_i u_i/3)^{1/2}$, rms velocity of the flow; $\langle\epsilon\rangle$, energy dissipation rate; $L = \tilde{u}^3/\langle\epsilon\rangle$, energy input length scale; $\eta = (\nu^3/\langle\epsilon\rangle)^{1/4}$, Kolmogorov length scale; $\tau_\eta = (\nu/\langle\epsilon\rangle)^{1/2}$, Kolmogorov time scale. ν is the fluid kinematic viscosity and is $1.75 \times 10^{-6} \text{ m}^2/\text{s}$.

R_λ	\tilde{u} (mm/s)	$\langle\epsilon\rangle$ (mm ² /s ³)	L (mm)	η (mm)	τ_η (s)
150	30.4	319	87.9	0.36	0.074
210	62.8	2800	84	0.21	0.025

The rotation rate vector of rods, $\dot{\mathbf{p}}$, is measured from quadratic fits to the measured orientations along trajectories versus time. The measurements are at two different Taylor Reynolds numbers ($R_\lambda = 150, 210$). We have done parallel experiments with tracer particles to measure the turbulence parameters. From measured tracer velocities, we extract the third order longitudinal structure functions and obtain the energy dissipation rate $\langle\epsilon\rangle$ from Kolmogorov's 4/5 law. Flow parameters are shown in Table I.

Figure 1 shows the probability distribution function (PDF) of the rotation rate squared, $\dot{p}_i \dot{p}_i$, normalized by the mean for different rod lengths. The PDF shows only a weak dependence on the rod length. The probability of rare events is somewhat smaller for long rods ($l/\eta > 20$) than for tracer rods ($l/\eta < 7$); however, this difference is only slightly larger than the measurement uncertainty due to the smaller number of samples for long rods. The error bars represent the random statistical error and the systematic error in measuring the rotation rates. Qualitatively,

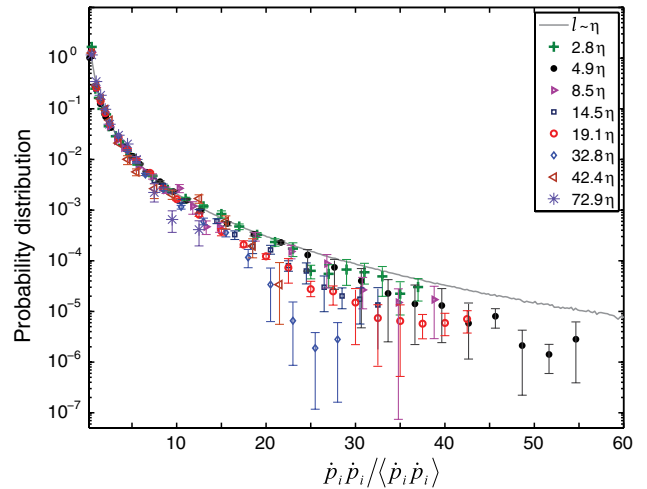


FIG. 1 (color online). The PDF of the rotation rate squared for different rod lengths. The lengths of rods are $l/\eta = 2.8$ (green crosses), 4.9 (black filled circles), 8.5 (right triangles), 14.5 (open squares), 19.1 (red open circles), 32.8 (blue diamond), 42.2 (brown left triangles), and 72.9 (purple asterisks), and tracers from simulation (solid gray line). The results are reported from two experiments at $R_\lambda = 150$ and 210 . The simulations [18] are for tracer rods at $R_\lambda = 180$.

the rotation rate PDF depends on rod length in the same way that the acceleration PDF for large spheres depends on the diameter [12].

The mean square rotation rate for different rod lengths is shown in Fig. 2(a). The measurements show smaller rotation rates for longer rods as expected since longer rods should begin to filter out the contributions from eddies smaller than their length. Figure 2(a) also shows the mean square rotation rate for randomly oriented rods predicted from Eq. (2) using our experimental measurements of R_{NN} at $R_\lambda = 150$ and 210. The measured mean square rotation rate is much smaller than the prediction for randomly oriented rods of the same length (l/η). However, this difference decreases as the length of the rod is increased. Previous studies of tracer rods [15,17,18,29,30] have shown that as rods are carried by the flow their orientation becomes correlated with the directions defined by the velocity gradient tensor. This alignment results in the suppression of the rotation rate of short rods compared to randomly oriented rods [18]. The smaller differences between the measured rotation rates of long rods and randomly oriented rods suggests that the alignment is slightly weaker for long rods.

Figure 2(b) shows the inertial range scaling from Eq. (3) with $C_2 = 2.0$ and compares it with the experimentally measured rotation rates and the prediction of Eq. (2) for randomly oriented rods using the measured velocity correlation function. Both the measured rotation rates and the prediction of Eq. (2) approach an $l^{-4/3}$ scaling for large l . The mean square rotation rates measured experimentally have smaller coefficients than the prediction of the $l^{-4/3}$ scaling due to the alignment of rods with the directions defined by

velocity gradients of the flow. For comparison we also show the results of simulation of rods at $R_\lambda = 53$ by Shin and Koch [17] in Fig. 2(b). This simulation also approaches the $l^{-4/3}$ scaling in the same range of rod lengths. For short rods, the experiments are somewhat above the simulations. This may be a result of different forcing which could be significant at these low Reynolds numbers, or it may reflect errors in the measured energy dissipation rate.

For $l > 30\eta$ in Fig. 2(b), one could fit the data with a different exponent slightly steeper than $l^{-4/3}$ scaling within the error bars of the experimental data. In this same range, the prediction of Eq. (2) is also steeper than $l^{-4/3}$. The cause of the steeper scaling can be found in the fact that the prediction of Eq. (2) overshoots the power law scaling in the range $20\eta < l < 50\eta$. This overshoot occurs in the range of scales slightly larger than the dissipative range because scales smaller than the length of the rod contribute to the rotation rate. The simulation results from Ref. [17] in Fig. 2(b) do not appear to have a steeper slope than the $l^{-4/3}$ scaling. However, at the Reynolds number of that simulation, the integral length scale is only 28η , so it is difficult to separate the effects of the forcing. We have used Batchelor's parametrization [31,32] of the structure function at a very high Reynolds number to remove the effects of the limited inertial range for R_{NN} in the prediction of Eq. (2). Figure 2(c) compares the prediction of Eq. (2) using Batchelor's parametrization with the $l^{-4/3}$ scaling from Eq. (3). The agreement is nearly perfect for rod lengths longer than 100η , well in the inertial range. The prediction using Batchelor's parametrization has the same overshoot for rods between $20\eta < l < 100\eta$ that we see in the experimental data.

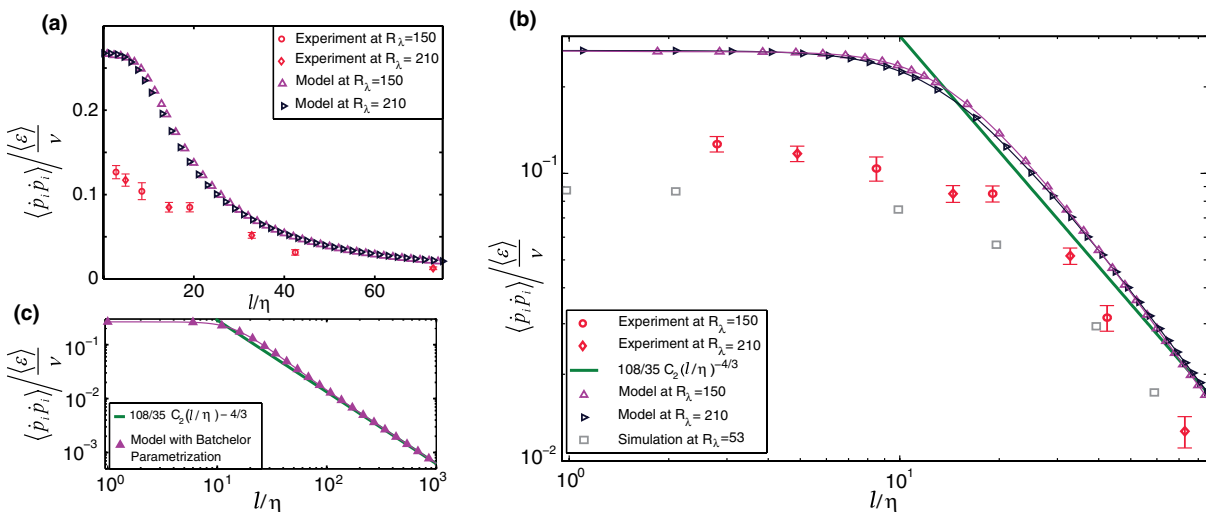


FIG. 2 (color online). Mean square rotation rate as a function of rod length. (a) Comparison of the experimental data at $R_\lambda = 150$ (red open circles) and 210 (red diamonds) with the model of randomly oriented rods at $R_\lambda = 150$ (purple up triangles) and $R_\lambda = 210$ (black right triangles). (b) Comparison of the mean square rotation rate of rods (red open circles and diamonds) and the model for randomly oriented rods (up and right triangles) with the $l^{-4/3}$ inertial range scaling law (solid green line) and the simulation by Shin and Koch [17] (grey squares). (c) Comparison of the inertial range scaling law (green solid line) with the model for randomly oriented rods using Batchelor's parametrization for very large Reynolds number (purple triangles).

The slightly steeper scaling of the rod rotation rate is similar to the effect observed in Ref. [12] for the accelerations of spheres with diameters in the inertial range. They argue that intermittency effects are responsible for the difference between their measured scaling and the prediction of dimensional analysis. It is possible that intermittency effects also play a role for rods. However, the availability of a theoretical foundation for calculating the rotation rates of long rods suggests another possible explanation due to the effects of dissipation range scales. As shown in Fig. 2(c), the overshoot occurs even when using Batchelor's parametrization which has no intermittency effects. It is possible that spheres also have an overshoot caused by dissipation range scales which leads to the observed scaling.

To measure the mean square rotation rate, we use the extrapolation method developed in Ref. [9] to remove the dependence on the smoothing used to measure derivatives. We have performed a simulation of the detection process similar to Ref. [9] and find the extrapolation overestimates the mean square rotation rate by 6% which we correct by a 6% shift. The error bars in Fig. 2 represent both the systematic error from extrapolation and the random error measured by analyzing subsets of the data. The random error is a larger fraction of the rotation rate for longer rods as seen in Fig. 2(b) due to the smaller number of samples.

Figure 3(a) shows the Lagrangian autocorrelation of the rotation rate measured for different rod lengths. Our measurements show that the correlation time of the rotation rate increases with rod length. Similar autocorrelation functions were obtained in simulations [17] at $R_\lambda \leq 53$. We expect that if the rods are rotating due to eddies of their size l , then the decay time for the correlation of rotation rate should scale as the turnover time at the length of the rods. In Fig. 3(b) the horizontal axis (t) is normalized by τ_l , the time scale of eddies with length scale l . After this normalization, the Lagrangian autocorrelation of the rotation rate for all rod lengths collapse on a single curve within measurement uncertainty. The time scales for short tracer rods ($l/\eta < 5$) is the Kolmogorov time scale (τ_η) and the time scales for longer rods are measured from longitudinal second order velocity structure function of the fluid particles [$\tau_l = \frac{1}{\sqrt{15}} l / \delta u_l = \frac{1}{\sqrt{15}} l / \sqrt{D_{LL}(l)}$]. Measuring the autocorrelation function for long rods ($l = 42.4\eta$ and 72.9η) is difficult because the rods span a significant fraction of the detection volume and so the trajectories are not long enough to measure long time autocorrelations. The collapse seen in Fig. 3(b) provides additional evidence, beyond that seen in the mean square rotation rate data, that rod rotations are controlled by eddies with size near the rod length.

Long rods provide a promising path for studying the dynamics of large particles in turbulence. For rods, slender body theory can be used to connect particle motion with the fluid flow even for particles much larger than the Kolmogorov scale while the analytical results for spheres are only available for small deviations from the small

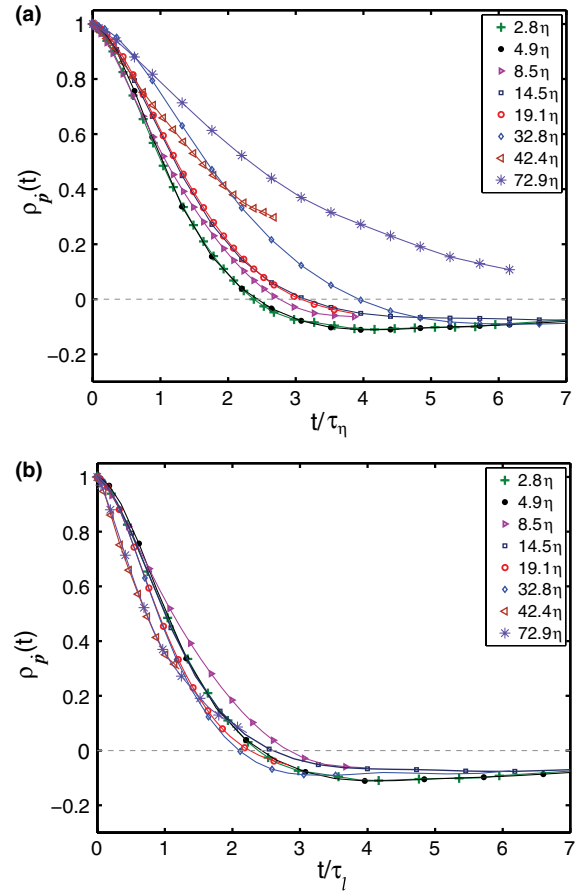


FIG. 3 (color online). Lagrangian autocorrelation of the rotation rate for different rod length. The lengths of rods are $l/\eta = 2.8$ (green crosses), 4.9 (black filled circles), 8.5 (right triangles), 14.5 (open squares), 19.1 (red open circles), 32.8 (blue diamond), 42.2 (brown left triangles), and 72.9 (purple asterisk). (a) Time is normalized by the Kolmogorov time. (b) Time is normalized by the turnover time of eddies with sizes equal to the length of the rods, τ_l . The symbols are displayed at every other data point.

particle limit. We have presented measurements of the rotations of rods with lengths extending well into the inertial range, and find that the mean square rotation rate approaches the $l^{-4/3}$ scaling that we predict from inertial range scaling of the velocity structure functions. The analytic prediction of rod rotation rate from the measured structure functions allows a new insight concerning the way the mean square rotation rate overshoots the scaling law for scales between the dissipation and inertial range. The PDF of rotation rate shows only a weak dependence on rod length. We find that rods develop preferential alignment so that their rotation rates are significantly smaller than that predicted for randomly oriented rods. The Lagrangian autocorrelation time of the rotation rate depends on the length of rods and scales with the eddy turnover time at a scale equal to the rod length.

Shin and Koch [17] provided a ground breaking simulation data set on this problem, but were limited to

$R_\lambda \leq 53.3$ where there is no considerable inertial range. A future numerical simulation at high Reynolds number using their method of simulating long fibers offers the possibility to study the motion of inertial range rods while also having access to the full velocity field around the rods. Experimental tracking of long rods in turbulence allows access to the dynamics of turbulent scales at the length of the particle from single particle measurements, and has potential to provide valuable information about Lagrangian dynamics as a function of the scale in complex turbulent flows.

We acknowledge support from NSF Grant No. DMR-1208990, and COST Actions MP0806 and FP1005. We thank Stefan Kramel for assistance in the experimental work and Enrico Calzavarini, Federico Toschi, Nicholas T. Ouellette, and Rui Ni for stimulating discussions.

*Corresponding author.
gvoth@wesleyan.edu

- [1] J. D. Bowen, K. D. Stolzenbach, and S. W. Chisholm, *Limnol. Oceanogr.* **38**, 36 (1993).
- [2] Marcos, J. R. Seymour, M. Luhr, W. M. Durham, J. G. Mitchell, A. Macke, and R. Stocker, *Proc. Natl. Acad. Sci. U.S.A.* **108**, 3860 (2011).
- [3] F. Lundell, D. Soderberg, and H. Alfredsson, *Annu. Rev. Fluid Mech.* **43**, 195 (2011).
- [4] G. Falkovich, A. Fouxon, and M. G. Stepanov, *Nature (London)* **419**, 151 (2002).
- [5] R. A. Shaw, *Annu. Rev. Fluid Mech.* **35**, 183 (2003).
- [6] F. Toschi, and E. Bodenschatz, *Annu. Rev. Fluid Mech.* **41**, 375 (2009).
- [7] E. Meiburg and B. Kneller, *Annu. Rev. Fluid Mech.* **42**, 135 (2010).
- [8] L. Biferale, E. Bodenschatz, M. Cencini, A. S. Lanotte, N. T. Ouellette, F. Toschi, and H. Xu, *Phys. Fluids* **20**, 065103 (2008).
- [9] G. A. Voth, A. La Porta, A. M. Crawford, J. Alexander, and E. Bodenschatz, *J. Fluid Mech.* **469**, 121 (2002).
- [10] N. M. Qureshi, M. Bourgoïn, C. Baudet, A. Cartellier, and Y. Gagne, *Phys. Rev. Lett.* **99**, 184502 (2007).
- [11] R. D. Brown, Z. Warhaft, and G. A. Voth, *Phys. Rev. Lett.* **103**, 194501 (2009).
- [12] R. Volk, E. Calzavarini, E. Leveque, and J.-F. Pinton, *J. Fluid Mech.* **668**, 223 (2011).
- [13] H. Homann, and J. Bec, *J. Fluid Mech.* **651**, 81 (2010).
- [14] E. Calzavarini, R. Volk, E. Leveque, J. F. Pinton, and F. Toschi, *Physica (Amsterdam)* **241D**, 237 (2012).
- [15] A. Pumir, and M. Wilkinson, *New J. Phys.* **13**, 093030 (2011).
- [16] S. Parsa, J. S. Guasto, M. Kishore, N. T. Ouellette, J. P. Gollub, and G. A. Voth, *Phys. Fluids* **23**, 043302 (2011).
- [17] M. Shin and D. L. Koch, *J. Fluid Mech.* **540**, 143 (2005).
- [18] S. Parsa, E. Calzavarini, F. Toschi, and G. A. Voth, *Phys. Rev. Lett.* **109**, 134501 (2012).
- [19] M. Parsheh, M. Brown, and C. Aidun, *J. Fluid Mech.* **545**, 245 (2005).
- [20] R. Holm and D. Soderberg, *Rheol. Acta* **46**, 721 (2007).
- [21] J. Lin, S. Zhang, and J. A. Olson, *Eng. Comput.* **24**, 52 (2007).
- [22] P. H. Mortensen, H. I. Andersson, J. J. J. Gillissen, and B. J. Boersma, *Phys. Fluids* **20**, 093302 (2008).
- [23] C. Marchioli, M. Fantoni, and A. Soldati, *Phys. Fluids* **22**, 033301 (2010).
- [24] J. Olson, and R. Kerekes, *J. Fluid Mech.* **377**, 47 (1998).
- [25] E. Calzavarini, R. Volk, M. Bourgoïn, E. Leveque, J. F. Pinton, and F. Toschi, *J. Fluid Mech.* **630**, 179 (2009).
- [26] S. B. Pope, *Turbulent Flows* (Cambridge University Press, Cambridge, 2000).
- [27] C.-C. Chien, D. B. Blum, and G. A. Voth, *J. Fluid Mech.* **737**, 527 (2013).
- [28] D. B. Blum, S. B. Kunwar, J. Johnson, and G. A. Voth, *Phys. Fluids* **22**, 015107 (2010).
- [29] S. S. Girimaji and S. B. Pope, *J. Fluid Mech.* **220**, 427 (1990).
- [30] B. Luthi, A. Tsinober, and W. Kinzelbach, *J. Fluid Mech.* **528**, 87 (2005).
- [31] G. K. Batchelor, *Math. Proc. Cambridge Philos. Soc.* **47**, 359 (1951).
- [32] S. Grossmann, *Phys. Rev. E* **51**, 6275 (1995).